Chapter 20
Integration of SCR Functionality into Diesel Particulate Filters

Thorsten Boger

Notation

A_s	Parameter
c_p	Heat capacity
d_c	Collector diameter
d_h	Hydraulic diameter
d_{Pore}	Pore diameter
d_s	Soot particle diameter
D_{BM}	Diffusion coefficient Brownian motion
f_0	Friction factor
h	Heat transfer coefficient
k	Mass transfer coefficient
L_{ch}	Channel length
L_W	Effective wall thickness
p	Pressure
Pe	Peclet number
Q	Cumulative heat of reactions
R_j	Source term for reactions involving species j
t	Time
T	Temperature
u	Velocity
y	Volume or mole fraction
X	Soot load or concentration
ε	Porosity
ε_s	Void fraction of soot deposit
η	Viscosity

T. Boger (✉)
Corning Incorporated, Corning, USA
e-mail: BogerT@corning.com

Corning Environmental Technologies, Corning GmbH, Abraham-Lincoln-Str. 30, 65189 Wiesbaden, Germany

I. Nova and E. Tronconi (eds.), *Urea-SCR Technology for deNOx After Treatment of Diesel Exhausts*, Fundamental and Applied Catalysis,
DOI: 10.1007/978-1-4899-8071-7_20, © Springer Science+Business Media New York 2014

η_{BM} Unit collector efficiency Brownian motion
η_{Int} Unit collector efficiency interception
λ Mean free path
κ Permeability
ρ Density
ζ Constant

20.1 Introduction

Most modern diesel engine aftertreatment systems comprise functions to oxidize hydrocarbons and CO, reduce particulate emissions (mass and number), and reduce NOx enabling compliance with ever tightening regulations. A typical system layout based on SCR as a means to reduce NOx is shown in Fig. 20.1a. A diesel oxidation catalyst (DOC) is followed by a catalyzed soot filter (CSF) and the SCR catalyst. In most advanced systems targeting high NOx conversion rates, an ammonia slip catalyst is installed post SCR catalyst. The system shown in Fig. 20.1a is representative of the majority of medium and heavy-duty systems designed to meet EPA 2010 and EU VI regulations as well as for heavier diesel passenger cars [1–5]. In some cases the SCR catalyst is installed upstream of the DPF [6]. For heavier passenger cars certified for advanced regulations similar system configurations with SCR are common, while lighter vehicles use in most cases either engine-based approaches or lean NOx trap technologies, or combinations thereof. In all systems, the DOC provides primarily for oxidation of HC and CO as well as oxidation of NO to NO_2 to facilitate the low temperature, passive oxidation of soot in the DPF as well as to accelerate the SCR reactions. The DPF is reducing the particulate emissions in mass and number. In most cases, the DPF is coated with a light oxidation function to promote the oxidation of CO to CO_2 during active regenerations as well as to provide for additional NO to NO_2 oxidation, enhancing the passive regeneration of soot by NO_2 [7, 8] and enabling more favorable NO/NO_2 ratios for the downstream SCR component. The SCR catalyst reduces NOx emissions using ammonia as reducing agent, typically derived from urea. Due to the potential of high temperatures post DPF, originating primarily from uncontrolled soot regenerations, zeolite-based SCR catalysts are often used in this configuration.

Although the configuration shown in Fig. 20.1a has proven to provide good functionality, there long has been a desire to combine some of the aftertreatment functionalities into fewer, multifunctional components. Integration of the SCR function or at least part of it into the DPF, as shown in Fig. 20.1b, is one such example. This desire for integration of SCR functionality is driven by several factors. One common theme is the objective of reducing the total packaging volume consumed by aftertreatment components, which has been growing significantly since the introduction of EU 4/IV and EPA 2007 regulations. Another

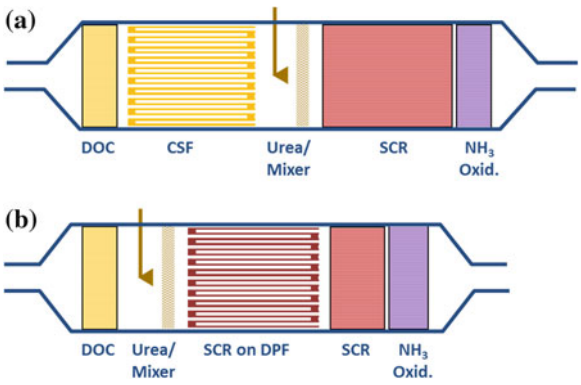

Fig. 20.1 Examples of diesel aftertreatment systems. **a** Conventional DOC-CSF-SCR system; **b** System with SCR integration into DPF

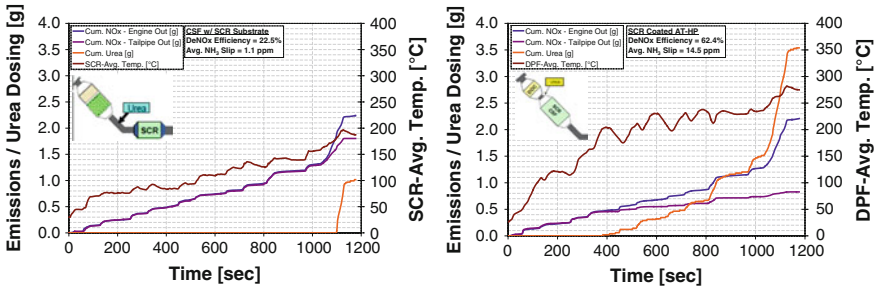

Fig. 20.2 Comparison of NOx emissions and SCR temperatures for a light-duty diesel application with (*left*) a CSF + SCR and (*right*) SCR integrated DPF system [9]

driver of significance, especially considering future light-duty regulations and engines with lower exhaust temperatures, is the need to move the SCR components closer to the engine enabling higher operating temperatures and deNOx efficiencies. An example demonstrating this benefit is shown in Fig. 20.2 [9]. In this example, the conventional system allows for urea dosing and deNOx not until the very end of the emission cycle. The system with the SCR catalyst integrated into the close coupled filter, on the other hand, enables urea dosing already fairly early in the cycle, providing for significantly higher deNOx efficiencies.

As common with all components that are designed to provide multiple functionalities we need to understand the trade-offs and compromises that have to be made to enable an optimized component and system. Objective of this contribution is to provide some of the basic considerations and fundamentals relevant to the combination of SCR catalysis and soot filtration. Since the general catalysis and function of the SCR catalyst is similar to the use in flow-through systems described in separate chapters of this book, the focus of this chapter will be on phenomena

that are introduced by the use of a particulate filter as substrate for the SCR catalyst. Examples of such phenomena are the impact of the accumulated soot and ash on the SCR reactions and vice versa, the pressure drop behavior of coated filters, the differences in the thermal robustness requirements compared to flow-through catalysts and, last but not least, the reduction of particulate emissions via filtration as additional emission relevant functionality of the integrated component.

20.2 Diesel Particulate Filter Technologies

Although diesel particulate filters (DPF) were first introduced in the 1980s, their widespread use started with the first introductions in some EU4 passenger cars in the early 2000s time frame, i.e., [10–13], followed by the introduction for heavy-duty systems in compliance with US EPA 2007 regulations, i.e., [14, 15]. Since the introduction of the EU5 regulation, DPFs have essentially become the standard in all light-duty applications designed to meet this regulation. For heavy duty, DPFs are used in most systems certified to meet US EPA 2007 and 2010 regulations. The introduction of the new EUVI heavy-duty standard is expected to lead to the same result, with DPFs being installed on all engines certified to this regulation. In the non-road sector, we currently find a mix of systems relying entirely on DOC and SCR as well as systems that use a DPF as well [16].

In the following sections particulate filter technologies will be discussed in general and with respect to the unique needs for SCR integration. Since coating technologies for filters are somewhat different from those used for flow-through substrates and have a significant impact on the performance of the composite filter-catalyst component, some general discussion will be dedicated to this topic as well.

20.2.1 Diesel Particulate Filter Designs and Materials

Although a number of designs have been proposed over the years the dominating filter design used by the majority of applications is the wall-flow filter shown schematically in Fig. 20.3. The filter is made of an extruded honeycomb structure with walls made of a porous refractory ceramic. The channels are plugged in a checkerboard pattern at alternate ends. This results in a pattern that force the exhaust flow from the inlet channels, through the porous walls into the outlet channels. On the path through the porous wall particulates are removed by filtration.

Different refractory ceramics are used for the filter matrix. Most common are cordierite-, aluminum titanate-, and silicon carbide-based products [15, 17–21]. Typical physical properties for these materials are provided in Table 20.1. All materials can withstand very high temperatures. Key differences between these

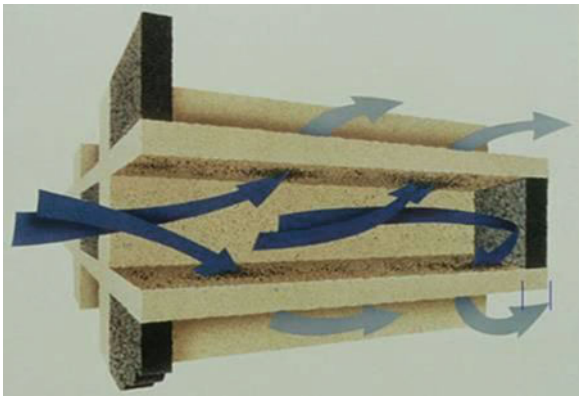

Fig. 20.3 Wall-flow diesel particulate filter design

Table 20.1 Physical properties of common diesel particulate filter materials [18]

	Aluminum titanate composition	Cordierite composition	Silicon carbide
Intrinsic material density, g/cm^3	3.40	2.51	3.24
Specific intrinsic heat capacity, J/(g K) (500 °C)	1.06	1.11	1.12
Volumetric heat capacity[a]; J/(cm^{3}K) (500 °C)	3.60	2.79	3.63
Coefficient of thermal expansion; 10^{-7}/ °C	~10[b]	~6[c]	~45[b]
Thermal conductivity; W/mK (500 °C)	~1	~1	~12

[a] Based on the material. Does not include porosity
[b] Measured between 25 and 1000 °C
[c] Measured between 25 and 800 °C

materials are (1) the thermal expansion, which is very low for the two oxides, cordierite and aluminum titanate, (2) the thermal conductivity, which is low for the oxides and higher for SiC and (3) the elastic modulus, which is low for the oxides providing robustness under thermal gradients.

In general, similar processes are used to manufacture the different filter technologies. The raw materials are batched and adjusted for their rheological properties enabling extrusion of the honeycomb matrix. This is followed by drying and high temperature firing. Materials such as cordierite and aluminum titanate are available in extruded, monolithic shapes up to very large diameters, enabled by their low thermal expansion and ability to withstand thermal stresses. SiC products have higher thermal expansion and require the use of segmenting techniques in which small extrudates are assembled, cemented, and contoured into the final filter product. In the final filter product, these segment seams typically reduce the available volume and area for filtration by ~5–8 % compared to a monolithic design. Another process step required for all materials is the plugging of the alternate channels.

Depending on the specific application, filter products with different levels of porosity and pore size are available. Porosities in the range of 40 % to roughly

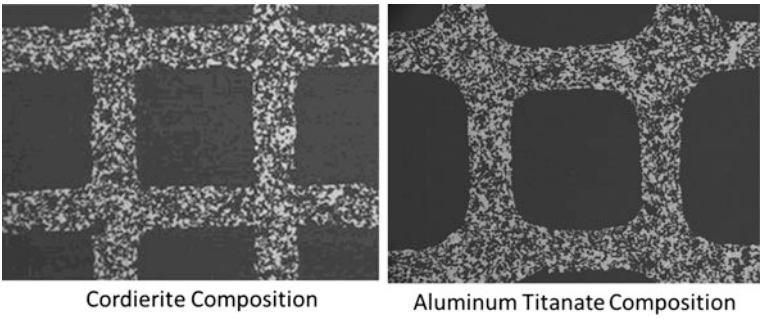

Fig. 20.4 SEM of honeycomb wall of high porosity cordierite (*left*) and aluminum titanate filters (*right*)

65 % are currently used for diesel particulate filters. As will be discussed later, most favorable for SCR integrated filter applications are filters with high porosity of 55 % or more. Figure 20.4 shows examples of SEM images taken from high porosity cordierite and aluminum titanate filter samples. An important feature that can be seen from these images is the excellent connectivity of the pores.

The pore size of diesel particulate filters is significantly larger compared to substrates used for flow-through catalysts. Most common are mean pore sizes in the range of 10–25 μm, compared to 2–5 μm for common flow-through substrates. The choice of pore size is determined by the trade-off between filtration and pressure drop. With respect to filtration, smaller pore sizes enable higher filtration efficiencies. This has to be balanced by the negative effect of small pore sizes on the wall permeability and ease of washcoating. Filters designed for integrated SCR applications typically have mean pore sizes in the medium to upper end of the given range (15–25 μm), mostly driven by the challenge to achieve high catalyst loads.

With respect to the cell design, square cells dominate. Common cell densities are between 200 and 350 cpsi, with the 200 cpsi dominating in heavy duty and the 300–350 cpsi dominating light-duty applications. The difference in cell density is primarily determined by the anticipated soot load in use, with higher cell densities being favorable if higher soot loads are anticipated.

The web thickness of filters is typically in the range of 8–18 mils (1 mil = 1/1000 inch or 25.4 μm), with 10–13 mil being most common. Especially in light-duty applications, filters with asymmetric cell design for increased specific ash storage have become widely used [22]. In these filters the cross-section of the inlet channels is increased by moving the cell webs toward the outlet channels. An example of a filter with such an asymmetric design is shown in Fig. 20.5 in comparison to a standard cell design filter. Various commercialized designs with asymmetric cell structures are available, e.g., ACT® (asymmetric cell technology), Octosquare, etc.

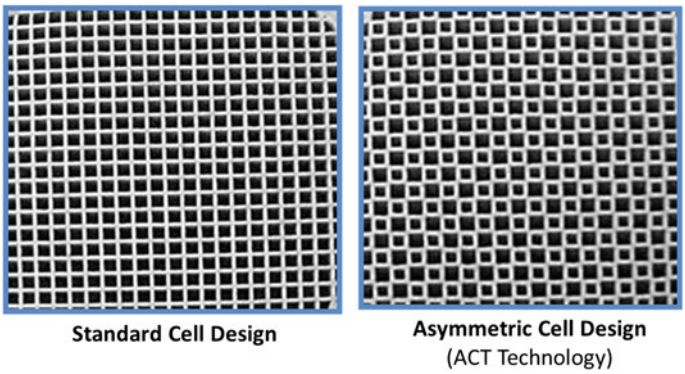

Fig. 20.5 Picture of a diesel particulate filter with standard (*left*) and asymmetric (*right*) cell design

20.2.2 Catalyst Coatings for Diesel Particulate Filters

In flow-through catalysts the active phase is typically coated onto the geometric surface area of the ceramic substrate material in form of a washcoat layer. An example is shown in Fig. 20.6(left). The substrates used to facilitate this approach typically have low porosity of ~25–35 % and small pores of 2–5 μm. Flow is along the channels, low pressure drop, good mass transfer and catalyst performance is achieved by optimizing the web thickness, cell density, and coating layer thickness [23].

In filter applications the exhaust flow is from the inlet to the outlet channels across the filter walls, enabling effective filtration of particulates. This key difference in flow leads to different preferences with respect to the deposition and location of the catalyst coating. It has been observed that due to the small size of catalyst particles (e.g., zeolite crystals), being typically in the range of ≤1–5 μm, an on-wall coated catalyst layer deposited analogous to flow-through substrates can have very low permeability, resulting in high pressure drop. It is therefore more favorable to deposit the catalyst uniformly within the porous wall space, utilizing so-called in-wall coating technologies. To enable reasonable catalyst loadings with this method the above-mentioned high porosity filter technologies are used for SCR applications. An example of a zeolite coated filter is shown in Fig. 20.6(right).

From a high level, methods for coating filters are comparable to substrates. First, a slurry is prepared with the catalyst particles dispersed. The coating step can be done by immersion, waterfall, or vacuum assisted methods. Since the coating is done on plugged filters, requiring the slurries to flow from one channel to the corresponding opposite channel the properties of the slurries have to be adjusted, to facilitate the penetration of the slurry into the wall and prevent on-wall deposition. Examples of important parameters used to adjust the slurry properties are the solids load, the particle size, and the pH. The differences between open flow-through substrates and plugged filters also need to be considered during the blow

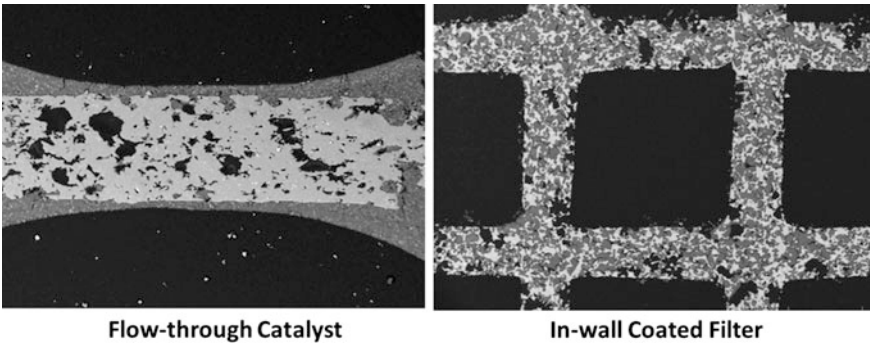

Fig. 20.6 Picture of an on-wall coated flow-through substrate (*left*) and an in-wall coated filter (*right*). Zeolite catalyst: *gray*; substrate/filter material: *white*; open pores: *black*

out step, during which excess slurry is removed. Final process steps are drying and calcining.

Comparing the maximum catalyst loadings on filters versus flow-through substrates, we find that filters are typically limited to about 65–85 % of what could be applied to a substrate, depending on the filter and coating technology. While for substrates the limit is usually determined by the adhesion of a thick layer of washcoat and the catalyst utilization, for filters it is primarily the available pore space for in-wall coatings and the associated increase in pressure drop when high washcoat loadings are applied. The latter effect will be further discussed in the next section.

20.3 Performance Considerations for SCR Integrated Diesel Particulate Filters

The performance of SCR integrated filters is characterized by the deNOx performance, analogous to catalysts based on flow-through substrates, combined with the additional requirements for the filter component, such as pressure drop, filtration, and thermal robustness under regeneration conditions. In addition, we have to consider the presence of soot and ash within the component and their influence on all the performance aspects including the reactions. In the following sections, each of these characteristics will be discussed in terms of basic fundamentals and design aspects.

20.3.1 Pressure Drop and Permeability

The pressure drop of a filter is an application critical parameter of significant practical relevance, impacting engine power and fuel consumption. In this section,

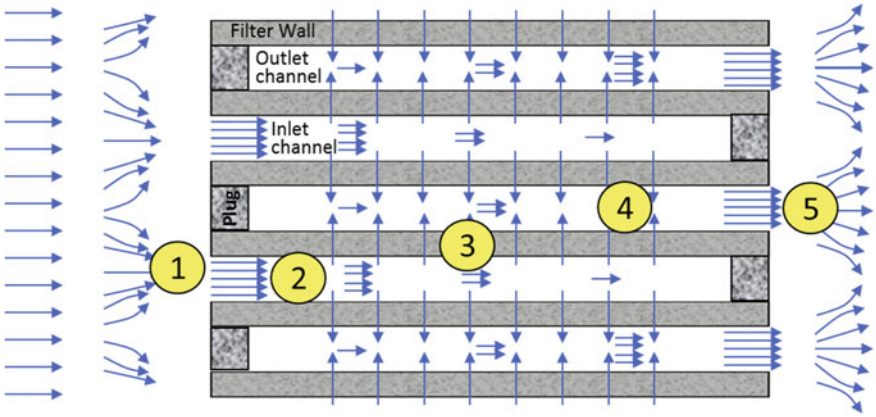

Fig. 20.7 Pressure drop contributions in wall-flow particulate filters

a brief description of the most relevant factors will be provided. There is a rich literature describing the modeling of the pressure drop of particulate filters in more detail. Examples are Refs. [24–26] and references therein.

The pressure drop of particulate filters is composed of five primary contributions, shown in Fig. 20.7. The inlet and outlet effects, shown as (1) and (5) in Fig. 20.7, are due to the contraction and acceleration as the gas enters the inlet channels and the expansion and deceleration of the gas as it exits the channels, respectively. Compared to flow-through substrates where inlet and outlet effects typically are less than 10 % of the total pressure loss, these pressure losses are larger in case of filters since only one half of the channels is open on each end. In addition, the open frontal area of filter honeycombs is often lower. For clean filters inlet and outlet effects can contribute as much as 30–40 % of the total pressure drop, especially at high flow rates. The turbulent entrance effects as result of the developing flow inside channels is typically lumped into these contributions. The inlet and outlet contributions are described by terms proportional to the kinetic energy, with the proportionality constant ζ_j.

$$\Delta p_j^{i/o} = \zeta_j \cdot \rho_j \cdot \left(u_j^{i/o}\right)^2$$

The index j represents filter inlet or outlet, and i/o indicates the condition at the inlet or outlet of the filter. Correlations for ζ are empirical and typically include the open frontal area as variable. Examples are provided in Refs. [27, 28]. In general the outlet effects roughly are two times larger than the inlet effects.

For the frictional losses along the inlet and outlet channels (Fig. 20.7, index 2 and 4) existence of a laminar flow profile is generally assumed within the channels. The pressure drop along the channels can therefore be described analogous to flow-through substrates.

$$\Delta p_{\mathrm{j}}^{\mathrm{ch}} = 2 \cdot f_0 \cdot \eta \cdot \frac{L_{\mathrm{ch}}}{d_{\mathrm{h}}^2} \cdot u_{\mathrm{j}}^{\mathrm{ch,eff}}$$

The index j again represents the inlet and outlet channels. η, L_{ch}, and d_{h} represent the viscosity, effective channel length, and hydraulic diameter, respectively. The friction factor f_0 is equal to 14.2 for a square channel. With respect to the velocity to be used it has to be considered that at the inlet side (region of inlet plugs), all the flow is in the inlet channels, whereas the opposite is true on the outlet side (region of outlet plugs), with all the gas flow exiting via the outlet channels. Hence, the local flow rate in the inlet and outlet channels varies along the length, which has to be considered in the choice for $u_{\mathrm{j}}^{\mathrm{ch,eff}}$. To illustrate this, examples for the simulated axial velocity profiles in the inlet and outlet channel as well as across the filter wall are shown in Fig. 20.8. The different lines represent the velocity profiles at different time steps during a soot loading process. Initially no soot is present and the wall permeability is high. The resulting axial velocity profiles are nonlinear. As soot is accumulated the effective wall permeability is reduced and the resistance across the wall and soot layer starts to dominate. This yields to an almost uniform wall-flow velocity and linear velocity profiles along the inlet and outlet channels.

The last contribution to pressure drop comes from the resistance to flow across the filter wall (index 3 in Fig. 20.7), from the inlet to the outlet channels. It is worth noting that this is the only contribution which is determined by the porous microstructure of the filter. In general the pressure drop across the wall can be described by Darcy's law.

$$\Delta p^{\mathrm{w}} = \eta \cdot \left(\frac{\Delta L_{\mathrm{w}}}{\kappa} \right)_{\mathrm{eff}} \cdot u^{\mathrm{w}}$$

with ΔL_{w} as effective thickness, κ as permeability, and u^{w} as wall-flow velocity. It should be mentioned that in some references a second-order term (Forchheimer term) is considered as well. However, under most practical terms this term is small and can be neglected. The permeability of a clean wall is in general a function of the porosity, the pore size distribution, and the general morphology of the porous wall, considering for example the connectivity of the pore network. The simplest approaches to estimate the permeability are based on correlations utilizing the porosity and mean pore size only, as described for example in [29, 30].

$$\kappa_{\mathrm{w}} = \frac{3}{200} \cdot \varepsilon \cdot \hat{d}_{\mathrm{pore}}^2$$

Here, κ_{w} is the wall permeability, ε the porosity and $\hat{d}_{\mathrm{pore}}$ the mean pore diameter. These correlations can provide reasonable estimates for the permeability of clean, uncoated filter walls. Typical permeabilities are in the range of $\kappa_{\mathrm{w}} = 1\text{–}6 \times 10^{-12}$ m^2. Coating of the porous filter wall with a catalyst changes the microstructure. The catalyst particles consume some of the pore space and change the effective microstructure. In addition, since the coating process has

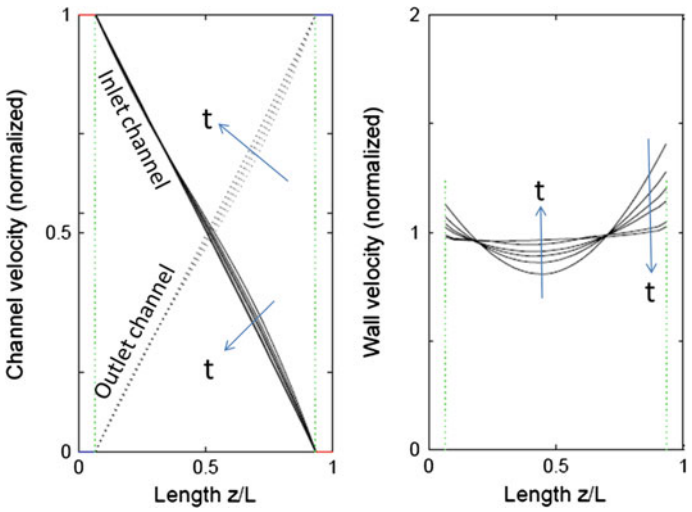

Fig. 20.8 Axial channel flow velocity (*left*) and wall-flow velocity (*right*) distribution at different time steps during soot loading of an initially clean DPF under steady-state flow conditions. The progression in time *t* is indicated by *arrows*

some directionality the use of bulk properties is less effective. In general, we observe a decrease in clean permeability that can often be described empirically by a power law or exponential function. A useful variable capturing the effect of coating in such a correlation is the ratio between the volume of the coating applied and the total pore volume available. This does, however, require the knowledge of the washcoat packing density, which is not easily accessible. In Fig. 20.9 are examples for the pressure drop and permeability as function of washcoat loading for two different filter designs. Both have the same microstructure and comparable web thickness, but Design 1 has a higher cell density than Design 2. For both designs we can distinguish two distinct regions. For low washcoat loadings the pressure drop is independent of the washcoat loading. In this region the permeability is high enough that the resistance to flow across the wall is not limiting; the microstructure has no significant impact on the pressure drop. The pressure drop observed is determined primarily by the filter geometry and design, as can be seen by comparing the two designs. At higher washcoat loadings, the pressure drop increases corresponding to the decrease in permeability. In this range we also observe that the Design 2, favorable for lower washcoat loadings, shows higher sensitivity and beyond a certain loading level even exceeds the pressure drop of Design 1. This is explained by lower washcoat capacity and surface area of this design.

The collection and deposition of soot also changes the permeability of the filter wall and can lead to a significant increase in pressure drop. Examples are shown in Fig. 20.10. Here, we have to distinguish between the effect of soot deposited inside the porous microstructure (deep bed filtration) and soot deposited onto the channel

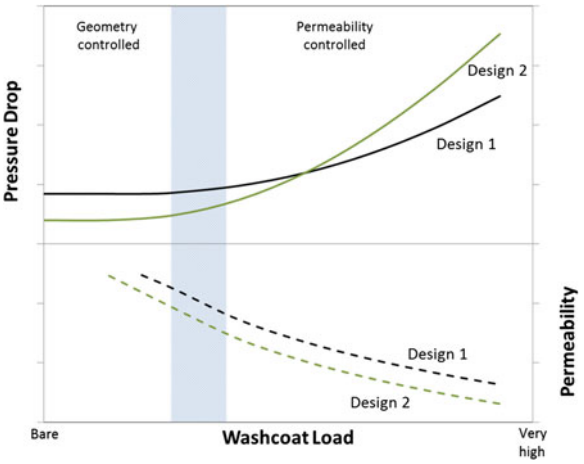

Fig. 20.9 Examples for the pressure drop and permeability of wall-flow particulate filter as function of the washcoat load. Data are for filters with two different cell designs

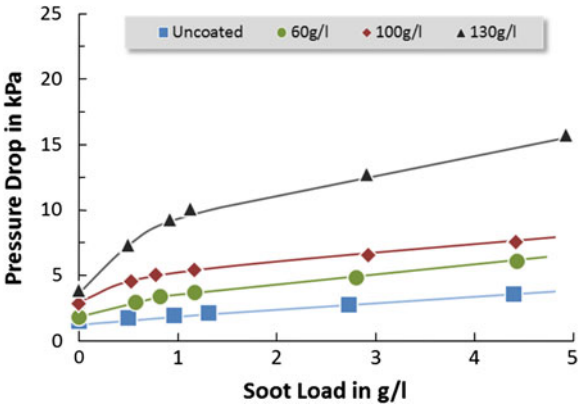

Fig. 20.10 Examples for the pressure drop of wall-flow particulate filter as function of the soot load. Lab pressure drop on 2″ samples with Printex U soot. Filter with Fe-ZSM-5 model coating

walls in form of a soot layer or soot cake. Soot deposited inside the microstructure can significantly reduce the wall permeability. Figure 20.11 illustrates this process showing how soot is deposited and accumulated in a synthetic microstructure, resulting in a decrease in effective permeability. This effect is observed already at low soot loads and is the result of the change in effective microstructure due to the deposition of soot combined with high local velocities inside the pore structure (for example, at pore necks, see Fig. 20.11). The latter amplify the effect of areas with increased resistance to flow. Advanced filter technologies with highly engineered microstructures address this effect and minimize the negative impact of soot deposited inside the microstructure. The effect of catalyst coating on the clean permeability was described above.

The effect of washcoating on the soot-loaded permeability can be even more significant. This can be seen from the comparison of the examples shown in Fig. 20.10. The difference in clean pressure drop is significantly smaller than the

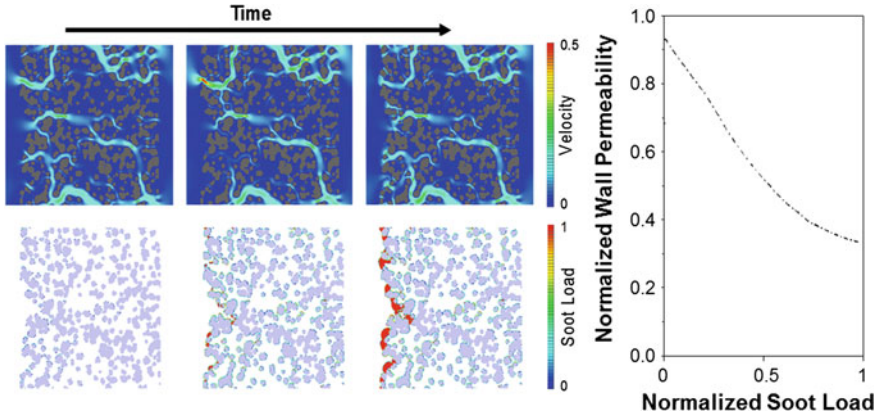

Fig. 20.11 Accumulation of soot inside the microstructure (*left*) and effect on permeability (*right*). Simulation results for a synthetic 2D microstructure with 64 % porosity and 18 μm mean pore size

difference in soot-loaded pressure drop. One explanation for this is that catalyst particles can deposit in the area of pore necks further restricting the flow.

Once a soot cake has formed on the wall surface, the further change in effective permeability of the wall/soot composite is determined to a large extent by growth of the low permeability soot layer. The soot permeability can be reasonably well described using the correlations provided for example in Refs. [29, 31, 32], with the Happel correlation being one example:

$$\kappa_{s,0} = \frac{3 - \frac{9}{2} \cdot (1 - \varepsilon_s)^{1/3} + \frac{9}{2} \cdot (1 - \varepsilon_s)^{5/3} - 3 \cdot (1 - \varepsilon_s)^2}{18 \cdot (1 - \varepsilon_s) \cdot \left(3 + 2 \cdot (1 - \varepsilon_s)^{5/3}\right)} \cdot d_s^2$$

This correlation should be combined with the Stokes–Cunningham correction, which considers slip as continuum laws for drag breakdown for very small particles under certain operating conditions.

$$\kappa_s = \kappa_{s,0} \cdot \left[1 + \frac{2 \cdot \lambda}{d_s} \cdot \left(1.257 + 0.4 \cdot \exp\left(-1.1 \cdot \frac{d_s}{2 \cdot \lambda}\right)\right)\right]$$

In these correlations, ε_s is the void fraction of the soot deposit, d_s the soot particle size, and λ the mean free path of the fluid. Soot deposits are typically very low in density (50–150 g/l), equivalent to soot void fractions of ~92–98 %, and have particles with an electrical mobility diameter in the range of 50–150 nm. As a result, the permeability of the soot layer is in the range of 10^{-14} m^2, more than two orders of magnitudes lower than the permeability of a clean wall.

Another parameter that needs to be considered with respect to pressure drop is the effect of ash. Particulate filters not only remove soot particles from the exhaust but also inorganic ash particles. These inorganic ash particles cannot be removed

during thermal regeneration but continue to accumulate over life. As a result, the volume and surface area available in the inlet channels decreases and the pressure drop increases. This has to be considered during the design and sizing of the filter. More details related to this consideration can be found for example in Refs. [28, 33].

To summarize the above details on pressure drop, the following generic design guidance may be used for SCR integration into a filter. With respect to cell design higher cell densities provide for larger filtration areas and lower wall-flow velocities. This can be beneficial for high soot loads or filters with very low coated permeability, but comes at the penalty of higher frictional losses in the absence of soot or low coating levels. With respect to the web thickness, thinner is in most cases favorable, but one has to ensure sufficient total pore volume for the catalyst coating (with the total pore volume being the product of porosity and wall volume). In addition, the mechanical strength of the filter component is a strong function of the web thickness. For the microstructure, higher porosities and larger pore sizes are favorable for higher permeabilities and coating capacity. This has to be traded off with the effect these variables have on mechanical strength, thermal robustness, and filtration.

20.3.2 Filtration

Intrinsically, the removal of particles is the primary emission functionality of the filter component. Particles found in diesel exhaust are typically in the range of 30–150 nm (described by their electrical mobility diameter). The filtration of these very small particles occurs based on different mechanisms. The most relevant ones are deposition due to Brownian motion, interception, and, to a lesser extent, inertia effects. This is shown schematically in Fig. 20.12. The filtration based on Brownian motion is related to the random movement or diffusion of small particles relative to the fluid stream lines. Once a particle gets close enough to a solid surface it can deposit and is removed from the fluid stream. Interception occurs when a particle's trajectory passes within one particle radius of the collecting body. In such a case, the particle traveling along that stream line gets in contact with the body and may be collected there. Deposition as a result of inertia is relevant for large, heavy particles only, which do not follow the fluid steam lines. In Fig. 20.13 an example is provided, showing the filtration efficiency as function of the particle size. The "V-shape" of the filtration efficiency curve with very high efficiencies for very small and very large particles is due to the transition between the different collection mechanisms. Very small particles are collected with high efficiency as a result of their significant Brownian motion. This effect decreases as the particles become larger. Very large particles are collected due to their inertia or, more relevant, as a result of them intercepting with the filter media. The efficiency of these mechanisms decreases as they become smaller. In the intermediate range typically between 80 and 200 nm, a minimum in filtration efficiency

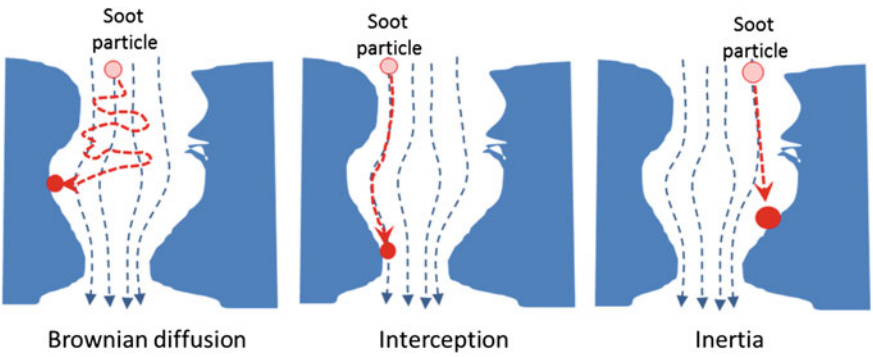

Fig. 20.12 Filtration mechanisms relevant for diesel particulate filters

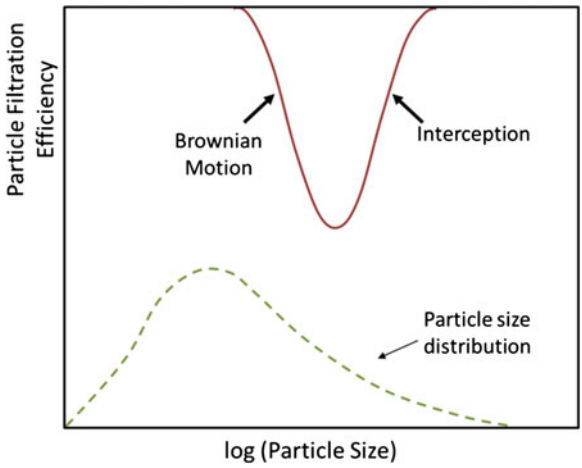

Fig. 20.13 Filtration efficiency as function of the particle size

is observed, resulting from the transition between the mechanisms. In the following paragraphs only brief descriptions of the physics describing these mechanisms will be provided. More exhaustive information can be found for example in [29–32, 34, 35] and the references therein.

Most models represent the porous filter wall as assemblage of unit collectors, onto which the soot particles are deposited. The size and number of the unit collectors can be derived from the mean pore size and porosity, for example, by assuming spherical shape.

$$d_c = \frac{3}{2} \cdot \frac{1-\varepsilon}{\varepsilon} \cdot \hat{d}_{\text{Pore}}$$

For these unit collectors the efficiency can be determined using established correlations, as given for example in [29–32, 34, 35]. For Brownian motion the unit collector efficiency η_{BM} can be described by [35]

$$\eta_{\mathrm{BM}} = 4 \cdot \frac{A_{\mathrm{s}}^{1/3}}{\mathrm{Pe}_{\mathrm{i}}^{2/3}} \cdot (1-\varepsilon)^{2/3}$$

With A_{s} being a parameter [35], primarily dependent on the porosity ε and Pe_{i} being the Peclet number. The Peclet number is proportional to the fluid velocity and the ratio between collector diameter d_{c} and diffusion coefficient for Brownian motion D_{BM}.

$$\mathrm{Pe}_{\mathrm{i}} = \frac{u_{\mathrm{w}}}{\varepsilon} \cdot \frac{d_{\mathrm{c}}}{D_{\mathrm{BM,i}}}$$

The particle size and temperature dependence of this collection mechanism is introduced via the Brownian diffusion coefficient, $D_{\mathrm{BM}} \sim (T/d_{\mathrm{s}}^2)$.

The collection of particles by interception can be described by [35]

$$\eta_{\mathrm{Int}} = 1.5 \cdot N_{\mathrm{r}}^2 \frac{[g(\varepsilon)]^3}{(1+N_{\mathrm{r}})^s}$$

where $g(\varepsilon)$and the power s are functions of the porosity and $N_{\mathrm{r}} = d_{\mathrm{s}}/d_{\mathrm{c}}$, providing the dependence on soot particle and collector size. Examples for how the clean filtration efficiency changes with pore size and porosity are shown in Fig. 20.14 for some reference conditions. The strong effect of the pore size can be seen as well as the counterintuitive effect of porosity, which is based on the increase in residence time for the particles within the wall. To assess the sensitivity of other filter design parameters such as web thickness, cell density, size, etc., on the clean filtration efficiency a simple characteristic parameter has been introduced in [36].

As soot is accumulated within the porous filter (see also Fig. 20.11), the filtration efficiency increases [30, 34–36]. The soot accumulated acts as a very efficient filtration medium due to its very small collector size and the fact that it is deposited in the areas of flow through the porous wall. Filtration efficiencies close to 100 % across the entire size spectrum are reached at very low soot loads. This is of significant practical relevance since in use a diesel particulate filter is rarely free of soot.

The effect of catalyst coating on filtration efficiency is not easy to generalize and depends on the type of coating applied, the uniformity, as well as the washcoat loading. An effect often observed in laboratory experiments with filters having high washcoat loadings as common for SCR integration is shown schematically in Fig. 20.15. The initial or clean filtration efficiency decreases as washcoat is added (Fig. 20.15b). This is explained by the shorter residence time within the partially filled pore space and more flow being directed through larger pores, which remain less filled with coating. The evolution of filtration as soot is loaded, on the other hand, is accelerated and very high filtration efficiencies are observed already at

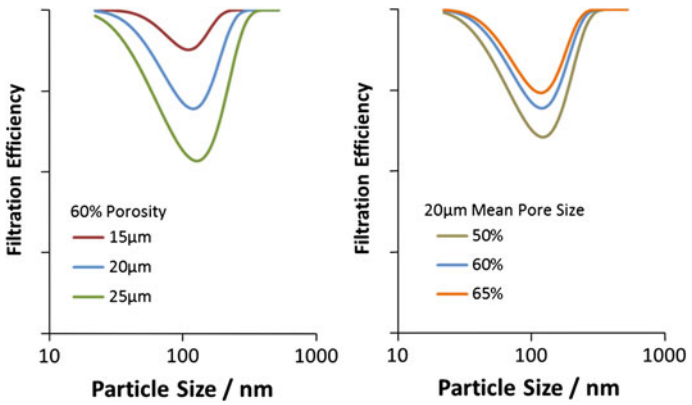

Fig. 20.14 Filtration efficiency as function of the mean pore size (*left*) and porosity (*right*). *Note* particle size is shown as electrical mobility diameter

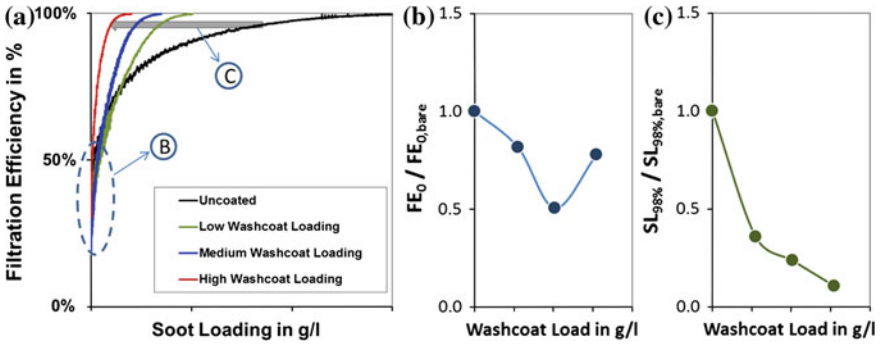

Fig. 20.15 Effect of washcoat loading on the filtration behavior. **a** FE versus soot load; **b** effect of washcoat on clean FE relative to uncoated; **c** effect of washcoat on soot load to reach 98 % FE relative to uncoated. *Note* Testing done at high space velocity to amplify effect

significantly lower soot loads (Fig. 20.15c). This is explained by the reduced pore volume that needs to be filled by soot to form an effective soot cake. With respect to practical applications, where commonly some soot is present, this can result in an observed improvement in filtration efficiency with coating, especially when significant quantities of SCR catalyst are applied.

20.3.3 Filter Regeneration, Thermal Management, and Durability

As described above, the accumulation of soot within the filter results in an increase in backpressure. This has negative impact on the power available and the fuel economy. To maintain the filter pressure drop within certain acceptable limits the soot has to be oxidized, which is commonly described as regenerating the filter. The interval after which the filter has to be regenerated is determined by the rate at which soot is accumulated and the maximum soot load that can be tolerated. For typical EU5 passenger cars the regeneration interval is typically in the range of 250–1500 km, depending on the engine raw emissions and the operating profile. City driving generally results in shorter intervals while highway driving enables longer intervals. Oxidation of soot is typically achieved by using either oxygen or nitrogen dioxide as oxidant [37–41].

$$C + \frac{1}{2}O_2 \rightarrow CO \quad (R1)$$

$$C + O_2 \rightarrow CO_2 \quad (R2)$$

$$C + NO_2 \rightarrow CO + NO \quad (R3)$$

$$C + NO_2 + \frac{1}{2}O_2 \rightarrow CO_2 + NO \quad (R4)$$

$$C + 2NO_2 \rightarrow CO_2 + 2NO \quad (R5)$$

While oxygen is abundantly available, the temperatures required to achieve appreciable reaction rates are >550 °C and rarely achieved under typical operation of diesel engines in light-duty and heavy-duty vehicles. Active measures are required to elevate the exhaust temperature to an appropriate level and this process is therefore called active regeneration. Examples for such measures applied to the engine controls are changes to the fuel injection timing, addition of late injections, intake air throttling, increase in load, etc. [42–45]. Typical duration of an active regeneration is 10–20 min, depending on the driving profile and conditions (transients, flow rate, temperature, etc.). Different approaches are used to monitor the accumulated soot mass and initiate active regenerations periodically. Examples of such monitoring and control strategies are provided in [42, 46–49]. Both open as well as closed loop methods are used. Open loop methods are either based on simple distance or time triggers or more advanced models, considering the engine-out soot emissions as function of the engine operation as well as the simultaneous oxidation of soot. Due to the lack of direct sensors, most closed loop strategies are based on a pressure drop measurement across the particulate filter. The signal combined with the calibrated correlation between pressure drop and soot load is then used to estimate the actual quantity of soot. In all cases an active regeneration request is triggered once a target soot load is observed.

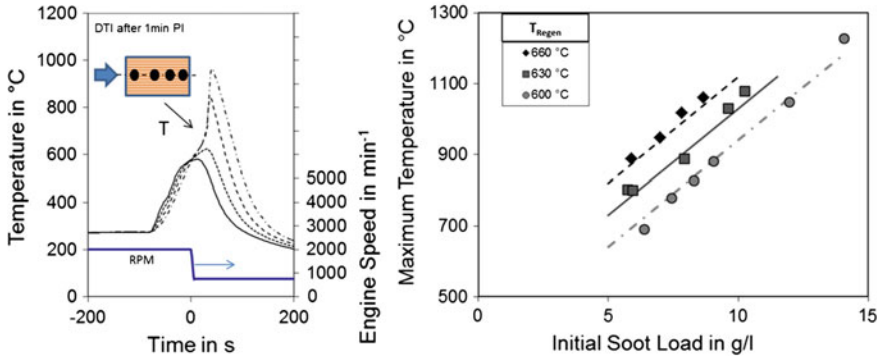

Fig. 20.16 Example of temperatures within an oxidation catalyst (Pt/Pd) coated DPF during a worst-case regeneration. *Left* temperatures at different axial locations; *right* maximum temperature as function of initial soot load and regeneration temperature

Typical exhaust gas temperatures during active regenerations are in the range of 550–650 °C, with most advanced strategies using lower temperatures during the initial phase of the regeneration and higher temperatures toward the end, i.e., [42, 45]. Such a staged or phased approach is essential to manage the heat release under the highly transient operating conditions observed on a vehicle. An example of a critical condition that can be observed is the case where a regeneration is just initiated, the soot oxidation has started, and then the engine changes to an idle operating mode. During engine idling, the exhaust flow rate is very low and the exhaust contains very high levels of oxygen. The abundance of oxygen results in the continuation of the soot oxidation, yet the low flow rate is insufficient to convectively remove the heat released [45]. As a result, the temperature within the filter can increase significantly. Examples of such a worst-case regeneration are shown in Fig. 20.16. The left diagram shows the transient evolution in local temperatures along the centerline of the filter, showing the rapid increase after the engine changed to an idle condition ($t = 0$ s). The right diagram shows examples for the dependence of the maximum temperature on the initial soot load as well as the exhaust (regeneration) temperature at start of the regeneration, before the change to engine idle. It should be mentioned that the temperatures observed are highly dependent on the conditions and the data shown are just examples for one set of parameters.

One important difference between typical DPF systems with oxidation catalyst coatings (containing Pt, Pd) and integrated SCR catalyst coatings is shown in Fig. 20.17 [9]. The heat release observed during a worst-case regeneration at a given soot load and condition is significantly higher for the oxidation coatings compared to integrated SCR technologies. This is a result of the effective catalysis of the oxidation of any CO formed during the soot oxidation (reaction R1 above). SCR catalysts show a significantly lower activity for such a CO oxidation and a

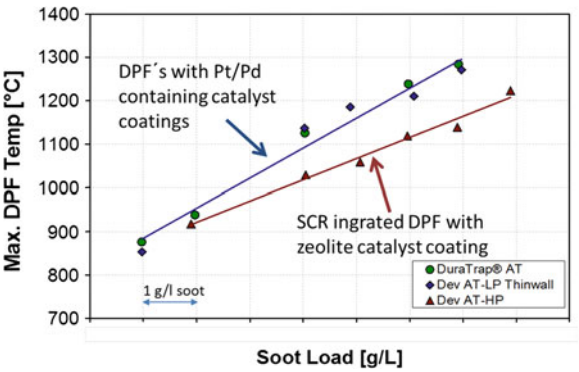

Fig. 20.17 Comparison maximum temperatures during worst-case regeneration conditions with different filter technologies. Adapted from [9]

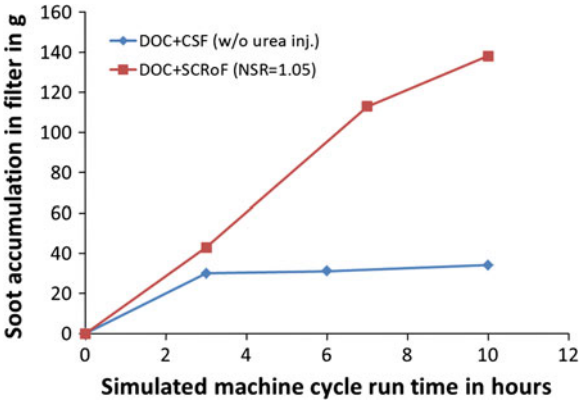

Fig. 20.18 Comparison of the soot load evolution of a DOC + CSF system versus a DOC + SCR on Filter (SCRoF) system under a transient engine operation. Data taken from [50]

significant fraction of the soot remains partially oxidized to CO, releasing less heat per mass of soot burned.

The oxidation of soot by NO_2 mentioned above occurs already at much lower temperatures of 300–550 °C, a range that can be observed during normal operation especially for heavy-duty applications. Since no active measure is required, this regeneration mechanism is called passive. For passive regeneration one limiting factor is the availability of NO_2. Most NO_x emitted by a diesel engine is in the form of NO. Typically, only a small fraction of 5–10 % is NO_2. To overcome this limitation some NO is oxidized to NO_2 over an upstream oxidation catalyst. In the case of oxidation catalyst coated filters, some of the NO_2 consumed by the soot oxidation is re-oxidized inside the filter wall and can be "recycled" via diffusion, further enhancing the passive regeneration rates. In case of SCR catalyst coated filters this latter mechanism does not occur. In addition, competition for NO_2 exists between the soot oxidation and the SCR reactions. This is shown in Fig. 20.18, taken from Ref. [50], in which the soot build up of a DOC + CSF is compared with a DOC + SCR on filter system. The CSF had a platinum containing coating and one can clearly see that a stable, low soot load is established after a short time

(balance point). For the SCR coated filter, this is not the case or would be expected at much higher soot loads. For light-duty applications, which typically do not rely on passive soot oxidation, this lower passive regeneration rate is not of major concern. For heavy-duty applications, however, this is of disadvantage and can result in penalties in fuel economy due to the higher operational soot and pressure drop levels as well as the need for more frequent active regenerations.

20.3.4 DeNOx Efficiency

The general catalysis of SCR catalysts applied to filter substrates is identical to the more conventional flow-through substrates. Differences exist with respect to the flow pattern, which includes flow across the catalyst coated porous wall in addition to the flow along the channels. Hence, transport of the reactive species occurs not only by diffusion from the gas bulk to the catalyst (as for flow-through catalysts) but also by means of a convective flow-through the catalyzed wall. The same is obviously true with respect to the heat transfer. For conventional flow-through catalysts, some effect of cell density can be observed, primarily at higher temperatures where mass transfer becomes limiting [23]. For filters, the range of cell densities used is significantly smaller ranging typically only from 200 to 350 cpsi and no significant effect has been reported so far.

The presence of soot accumulated in close proximity to the catalyst is another difference of filters with integrated SCR functionality leading to competition for NO_2. The NO_2 entering the filter can either react with accumulated soot according to the passive soot oxidation reactions mentioned above, (R3)–(R5), or the NO_2 can react within the SCR reaction system promoting, for example, the rate of deNOx via the fast SCR route, (R6).

$$NO + NO_2 + 2NH_3 \rightarrow 2N_2 + 3H_2O \qquad (R6)$$

Under most application conditions the rate of the SCR reactions exceeds the rate of the soot oxidation. This is especially true under low to medium temperatures as commonly found in light-duty emission cycles. Under these conditions, no difference in deNOx efficiency was observed between clean filters and filters loaded with 6–8 g/l of soot [51, 52], see Fig. 20.19. This was also shown in Ref. [53] under laboratory test conditions with a NO_2/NO_x ratio of 0. In the same study, either no effect of the presence of 5 g/l soot or a slightly reduced activity was reported for $NO_2/NOx = 0.5$ and temperatures above 200 °C. At a high NO_2/NO_x ratio of 1 a beneficial effect of soot was shown for temperatures below 275–300 °C [53]. This could be explained by some consumption of NO_2 reacting with soot according to (R3)–(R5) and changing the SCR reaction pathways toward the faster reactions involving NO and NO_2.

The amount of ammonia stored in the filter is of relevance to transient operation and cold start conditions. In [53], it was shown that despite its high surface area the

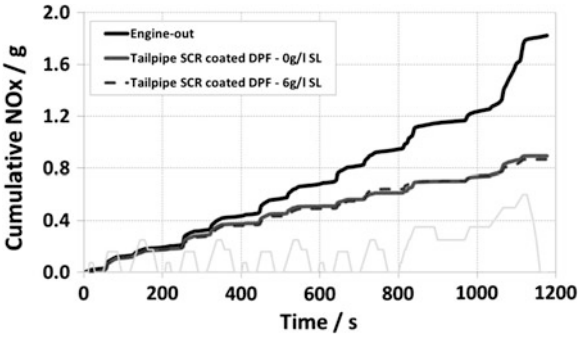

Fig. 20.19 Example of DeNOx efficiency over NEDC with a clean and a soot-loaded filter with integrated SCR catalyst, adapted from [51]. *Gray line* at the *bottom* indicates the vehicle velocity

soot stored in the filter adds no or only a negligible ammonia storage capacity. As mentioned above, over the life of the filter ash also accumulates within the inlet channels. The ash can deposit on the walls as well as in the rear of the filter in form of a plug. The ash plug in the rear of the filter can affect the deNOx efficiency since the wall-flow region with intimate contact between gas and catalyst is reduced and in the region of the ash plug mass transfer occurs by diffusion from the outlet channel to the wall only.

With respect to aging one has to distinguish between thermal aging and poisoning. Poisoning can be expected to be similar to flow-through catalysts with the additional potential for accumulated ash interacting with catalyst. With respect to the ash it should be mentioned that we typically do not see any significant ash quantities penetrating into the pore structure. Hence, if the coating is located inside the pores (or the outlet channel) the ash and catalyst will be spatially separated. The thermal exposure during active regenerations and the above-described worst-case conditions are significantly different from the conditions typically experienced by a standard flow-through SCR catalyst. This needs to be considered with respect to the selection of the catalyst, the selection of the filter technology and the durability evaluations. Typical durability testing with filters is done by performing a large number of regenerations and then test for filtration and deNOx performance. Most severe are repeated worst-case regenerations, for example, under the above described drop to idle conditions. Under these conditions, local peak temperatures inside the filter can be in the range of 1000 °C and more. The number of worst-case regenerations that should be used in these durability tests depends on the application. In [54], it was shown for several test vehicles that under normal operating conditions only a small fraction of regenerations actually lead to severe conditions. In general, the conditions are expected to be more severe in passenger car applications compared to heavy-duty applications, since the former experience often a more transient driving profile with higher soot loads as well as more frequent idling events. Figure 20.20 shows examples [51] for several zeolite coated filter samples exposed to a larger number of worst-case regenerations with peak temperatures in the range of 1100 °C. Similar data can be found in other references, for example [52]. The data demonstrate that advanced filter and

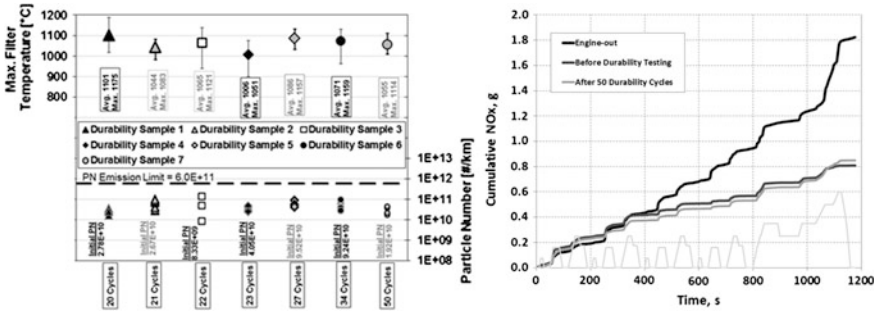

Fig. 20.20 Examples of durability test results over repeated worst-case regenerations with zeolite SCR catalyst coated high porosity aluminum titanate filter [51]

catalyst technologies can maintain low particulate emissions over such harsh conditions as well as maintain good deNOx activity. To understand the limited effect on catalyst activity shown in this example, it has to be mentioned that the temperature distribution within the filter during these extreme regenerations is highly nonuniform. The peak temperatures are observed in small regions, typically in the back of the filter, and for very short durations only [54]. As a result, the catalyst primarily deactivates locally with larger portions of the filter being aged at significantly milder conditions.

20.4 Modeling of SCR Integrated Particulate Filters

The modeling of particulate filter components has been described in a large number of publications. Examples are Refs. [36, 55–62]. In general, one has to distinguish between simple 0D models, treating the entire filter as one uniform body, and more detailed 1D up to 3D models. For pressure drop and filtration simulations, simple and fast 0D models are often sufficient and provide for an efficient engineering tool. The correlations that are used in these models have been described in the above sections. For some control algorithms, 0D models have been used to simulate the thermal behavior and the reactions occurring inside the filter, e.g., [45]. However, for a better understanding of the phenomena occurring inside the filter and more quantitative description 1D models, assuming uniform flow, temperature, and concentrations in the radial direction, have proven useful yet still efficient. Higher dimensional models are required to consider radial nonuniformities in flow, temperature, or soot loading. Since these models are computationally more expensive their use is typically limited to cases where the additional information is critical. We will limit the discussion to 1D models. In Fig. 20.21 a schematic of a filter with the relevant terms is shown. Due to the design of the filter, one has to distinguish between three axial regions, the two plug zones and the center of the filter representing the main part, and three phases, the

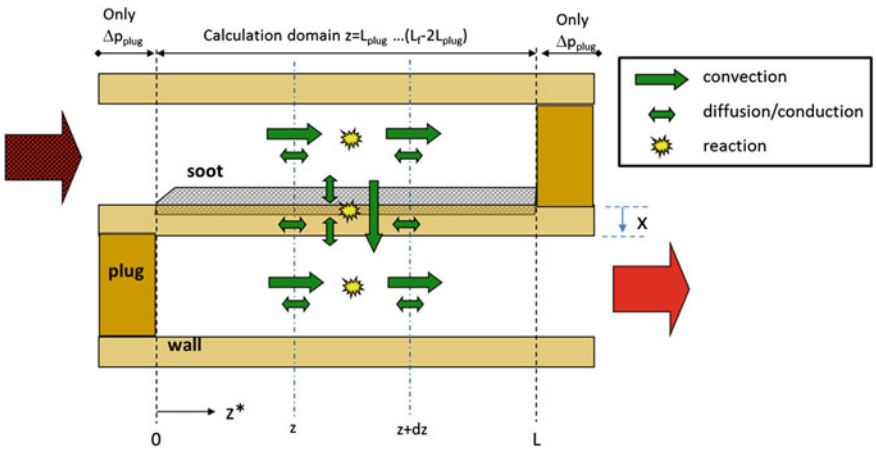

Fig. 20.21 Schematic of filter model

gas phase in the inlet and outlet channel and the wall (solid) phase. The latter phase also includes the soot deposited. The inlet and outlet plug regions can be described analogous to flow-through catalysts and will not be further discussed here. In the main filter region, the gas phase in the inlet and outlet channels is typically treated as locally uniform across the channel and the equations for conservation of mass, momentum, and energy apply. In the inlet channel, we further have to consider for the accumulation of soot (and ash) and the resulting change in the open channel area. The resistance of the flow across the soot layer is best considered in the equations describing the flow across the wall. The wall phase can be either treated as uniform from inlet channel to outlet channel surface or changes across the wall (x-direction in Fig. 20.21) can be considered. Convective flow within the wall in axial direction (z-direction) can typically be neglected, enabling the use of simpler 1D + 1D models, i.e., [36, 62]. The resistance to flow across the wall is described as Darcy flow by the local effective permeability, for which the correlations described in a previous section can be used. Although considered in some references, we have found that the contribution from the second-order term for wall-flow is typically small and can often be neglected. With respect to the source terms do conventional Sh- and Nu-numbers for square channels describe the diffusive/conductive mass and heat transfer between the gas and wall phases reasonably well. Reactions are considered where they occur, i.e., homogeneous gas phase reactions within the respective gas balance and catalyzed reactions within the wall phase equations. Soot oxidation is considered within the wall phase equations only. A summary of model equations for the example of a 1D description of the filter as described in Ref. [56] is provided in Table 20.2 with the notation adapted and the corresponding species equations added. Unlike the equations in [56] the effect of soot on the energy storage and axial thermal conductivity is neglected, since these contributions are

Table 20.2 Model equations (1D) for a wall-flow filter adapted from [56] and with species conservation equations being added

Conservation of mass	Inlet channel	$0 = -\frac{\partial}{\partial z}\left(d_\mathrm{i}^2 \rho_{\mathrm{g,i}} u_\mathrm{i}\right) - 4\mathrm{d}\rho_{\mathrm{g,w}} u_\mathrm{w}$
	Outlet channel	$0 = -\frac{\partial}{\partial z}\left(d_\mathrm{o}^2 \rho_{\mathrm{g,o}} u_\mathrm{o}\right) + 4\mathrm{d}\rho_{\mathrm{g,w}} u_\mathrm{w}$
Conservation of gas species	Inlet channel	$0 = -\frac{\partial\left(u_\mathrm{i} y_{\mathrm{g,i,j}}\right)}{\partial z} - \frac{4}{d_\mathrm{i}} u_\mathrm{w} y_{\mathrm{g,i,j}} + \frac{4}{d_\mathrm{i}} k_{\mathrm{i,j}}\left(y_{\mathrm{w,j}} - y_{\mathrm{g,i,j}}\right) + R_{\mathrm{i,j}}$
	Wall	$\varepsilon \frac{\partial y_{\mathrm{w,j}}}{\partial t} = \frac{4}{d_\mathrm{o}}\left(k_{\mathrm{i,j}} + u_\mathrm{w}\right)\left(y_{\mathrm{g,i,j}} - y_{\mathrm{w,j}}\right) + \frac{4}{d_\mathrm{i}} k_{\mathrm{o,j}}\left(y_{\mathrm{g,o,j}} - y_{\mathrm{w,j}}\right) + R_{\mathrm{w,j}}$
	Outlet channel	$0 = -\frac{\partial\left(u_\mathrm{o} y_{\mathrm{g,o,j}}\right)}{\partial z} + \frac{4}{d_\mathrm{o}} u_\mathrm{w} y_{\mathrm{w,j}} + \frac{4}{d_\mathrm{o}} k_{\mathrm{o,j}}\left(y_{\mathrm{w,j}} - y_{\mathrm{g,o,j}}\right) + R_{\mathrm{o,j}}$
Conservation soot	Wall	$\frac{\mathrm{d}x_\mathrm{s}}{\mathrm{d}t} = -\frac{4}{d_\mathrm{i}} y_{\mathrm{i,s}} \rho_\mathrm{s} u_\mathrm{w} + R_{\mathrm{w,s}}$
Conservation of energy	Inlet channel	$0 = -c_{\mathrm{pg,i}} \rho_{\mathrm{g,i}} u_\mathrm{i} \frac{\partial T_{\mathrm{g,i}}}{\partial z} + \frac{4d}{d_\mathrm{i}^2} h_\mathrm{i}\left(T_\mathrm{w} - T_{\mathrm{g,i}}\right)$
	Wall	$c_{\mathrm{p,w}} \rho_\mathrm{w} L_\mathrm{w} \frac{\partial T_\mathrm{w}}{\partial t} = h_\mathrm{i}\left(T_{\mathrm{g,i}} - T_\mathrm{w}\right) + h_\mathrm{o}\left(T_{\mathrm{g,o}} - T_\mathrm{w}\right) + \rho_{\mathrm{g,w}} u_\mathrm{w}\left(c_{\mathrm{pg,i}} T_{\mathrm{g,i}} - c_{\mathrm{pg,w}} T_\mathrm{w}\right) + \lambda_\mathrm{w} L_\mathrm{w} \frac{\partial^2 T_\mathrm{w}}{\partial z^2} + Q$
	Outlet channel	$0 = -c_{\mathrm{pg,o}} \rho_{\mathrm{g,o}} u_\mathrm{o} \frac{\partial T_{\mathrm{g,o}}}{\partial z} + \frac{4}{d}\left(h_\mathrm{o} + c_{\mathrm{pg,w}} \rho_{\mathrm{g,w}} u_\mathrm{w}\right)\left(T_\mathrm{w} - T_{\mathrm{g,o}}\right)$
Conservation of momentum	Inlet channel	$0 = -\frac{\partial p_\mathrm{i}}{\partial z} - \frac{\partial}{\partial z}\left(\rho_{\mathrm{g,i}} u_\mathrm{i}^2\right) - \frac{2 f_0 \mu_\mathrm{i} u_\mathrm{i}}{d_\mathrm{i}^2}$
	Wall	$0 = -\left(p_\mathrm{i} - p_\mathrm{o}\right) - \mu_\mathrm{w}\left(\frac{L_\mathrm{w}}{\kappa_\mathrm{w}} + \frac{d}{2\kappa_\mathrm{s}} \mathrm{In}\left(\frac{d}{d_\mathrm{i}}\right)\right) u_\mathrm{w}$
	Outlet channel	$0 = -\frac{\partial p_\mathrm{o}}{\partial z} - \frac{\partial}{\partial z}\left(\rho_{\mathrm{g,o}} v_\mathrm{o}^2\right) - \frac{2 f_0 \mu_\mathrm{o} u_\mathrm{o}}{d_\mathrm{o}^2}$

Note The contribution from soot on energy storage and thermal conductivity considered in [56] were neglected

typically small compared to the contributions of the filter solid. In the equations d is the channel diameter, ρ the density, u the velocity, c_p the heat capacity, T the temperature, h and k the heat and mass transfer coefficients, λ the thermal conductivity, μ the viscosity, L_w the wall thickness, κ the permeability, and f_0 the friction factor. The indices i and o denote the values for the inlet and outlet channels, respectively, and w and s the wall and soot phase. The model neglects thermal conductivity and axial diffusion in the gas phase and treats the gas phase in both channels as quasi-steady-state. For soot a common assumption is that it is retained within the wall with high filtration efficiency and in the equations of Table 20.2 an ideal filtration efficiency of 100 % is assumed. R_j represents the sum of all reactions involving species j and Q is the cumulative heat release upon all reactions occurring. As initial conditions the values at $t = 0$ s are used. Prior to the simulation it might be required to initiate the axial flow field. A boundary condition is that at $z/L = 0$ the mass flow is equal to the exhaust flow for the inlet channel, whereas it is zero in the outlet channel. The opposite is true for the outlet, $z/L = 1$, where the mass flow in the inlet channel equals zero and is equal to the exhaust flow rate in the outlet channel. The pressure boundary condition is defined at the outlet and is equal to the ambient pressure plus the pressure drop across any components downstream of the filter.

20.5 Application Examples

In this section, some of the published studies related to SCR integration into the particulate filter will be discussed. The discussion is separated into light-duty passenger car applications and heavy-duty or non-road applications.

20.5.1 Light Duty

The advantage of a more compact, packaging space reduced system is discussed in Refs. [63–66]. The systems used in these studies were all for heavier vehicles targeting primarily certification for US regulations. Lee et al. [63] discuss the potential and limitations of a system with Cu/Zeolite-based SCR catalyst integrated into the DPF for a pick up truck equipped with a 4.9 l prototype light-duty diesel engine. Filters with 200 and 300 cpsi were used. The observed NOx reduction for the integrated SCR/DPF technology was found to be comparable with that of the standard Cu-based flow-through SCR technology when tested over cold start FTP and US06. These results were found to be independent of the level of soot loading in the filter (tested up to 5 g/l). The authors did observe degradation in deNOx performance after experiments with active regenerations. Authors from the same group [9] report on an additional study in which they repeated up to 300 soot loading and regeneration cycles to simulate 120 k miles of operation. Regeneration was initiated at 4 g/l soot and a target temperature of 625 °C. The

deNOx efficiency of the aged systems decreased when compared to the fresh performance. The level of change depended on the technology and aging. The pressure drop of the integrated system was found to be higher compared to a conventional DPF plus SCR system. The maximum temperatures observed during worst-case drop to idle regenerations were about 100 °C lower compared to a CSF. The main benefit of the integrated system referenced is the reduced packaging volume. Cavataio et al. [65] discuss laboratory results obtained with different catalyst and filter technologies. In the laboratory tests, the coated filters showed comparable deNOx performance as conventional flow-through technologies. The higher backpressure was mentioned as a concern and area for improvement. In [66], the same group reports on promising results with integrated SCR on filter systems tested on a Land Rover with a 2.7 l V6 diesel engine. The system had both an SCR coated filter as well as a conventional SCR component. Placing the conventional SCR component upstream of the coated filter was found to be more favorable.

References [9, 51, 52, 67–69] discuss the advantage of integrated SCR-filter systems with respect to improved emissions performance in cold start cycles as result of the closer coupled location. Harth [67] reports on data of SCR integrated filter systems tested under light-duty conditions. The closer coupled location of the integrated system enables significantly lower NOx emissions over the NEDC compared to a conventional DPF plus SCR system. Excellent stability, comparable to a conventional system is shown over simulated 180,000 km with active regenerations every 800 km. Excellent stability under repeated regeneration conditions expected for light-duty systems is also shown in Refs. [51, 70]. Stiebels [52] and Boorse [68] show data on the sensitivity to NO_2/NO ratio entering the coated filter, with higher deNOx efficiencies at higher NO_2/NO_x ratios. In [69], the sensitivity with respect to the NO_2 ratio was reported to be low for the Cu-zeolite catalyst used. Ballinger et al. [71] show data for cordierite and SiC filters demonstrating comparable performance under hot test cycle conditions. Unfortunately no cold start cycle data were reported where a benefit of the lower thermal mass and lower thermal conductivity cordierite filter could be expected. The authors also show data comparing the pressure drop of zeolite coated filters with conventional oxidation catalyst coated filters (CSF); at low soot loads roughly 30 and 130 % higher values are shown for the SCR catalyst coated cordierite and SiC filters, respectively.

A commercial application has been reported by Volkswagen for some EU6 vehicle applications of their new 1.6 and 2.0 l TDI engines [72]. The system comprises a close coupled DOC followed in short distance by an SCR catalyst coated DPF. In addition, a slip catalyst with combined SCR and oxidation functionality is installed downstream of the DPF. The urea injection is located in-between the DOC and DPF components and a static mixer is used to improve distribution and evaporation within the limited space. Due to the high temperatures that can occur in this very close coupled position, a water-cooled urea injector was selected and the supply lines for the aqueous urea solution are made of highly temperature resistant materials.

20.5.2 Heavy Duty

The reduction in overall aftertreatment packaging volume as well as the potential for improved deNOx functionality as result of an increased SCR catalyst volume are the key features discussed in publications related to heavy-duty systems. In [73], Oladipo et al. demonstrate good conversion efficiency of SCR catalyst coated filters over several heavy-duty emission cycles. The performance, however, was slightly less compared to flow-through catalysts with the same catalyst. The authors observed that, with respect to the washcoat technologies considered, the effect on pressure drop is more relevant than the effect on conversion. Some of the technologies had pressure drop comparable to a reference CSF. The authors did observe some negative effect of soot on deNOx efficiency. Naseri et al. [74] discuss the concept of replacing the oxidation catalyst coated filter in a DOC + CSF + SCR system by an SCR catalyst coated filter to enable higher overall deNOx conversions. The total component volume as well as the flow-through SCR components were kept the same. The testing was done on a US 2007 heavy-duty engine. In case of the integrated SCR-filter system, the engine was operated without EGR at high engine out NOx emissions of 5 g/(hp h). The conventional system was tested at the same high NOx as well as at a level of 1–1.5 g/(hp h). At equal operating conditions, the system with integrated SCR-filter component provided better deNOx efficiency enabling operation at higher engine-out NOx and improved fuel economy. The authors also report that the integrated SCR-filter system demonstrated better passive regeneration capability under higher engine out NOx conditions as compared to the CSF system under lower engine out NOx. Tan et al. [75] report on a system consisting of two DOC's followed by a flow-through SCR component and then an SCR coated filter. In addition, a reference system with CSF in the same rear position was tested. The pressure drop results show a 48 and 52 % higher pressure drop for the SCR integrated filter compared to the CSF when tested clean and at 5.2 g/l soot, respectively. These values resulted in 9 and 18 % higher system pressure drop, respectively, but were still within the design targets for the system. The soot regeneration efficiency of the SCR coated filter was found to be slightly lower but was recovered by minor adjustments to the strategy. The emission tests showed the potential for an SCR volume reduction of 51 and 44 % for the US06 and HD FTP emission cycle. The opportunity for downsizing the aftertreatment equipment is also discussed in Refs. [76, 77] targeting EU VI heavy duty applications. The authors report high NOx conversion efficiencies as well as particle number emissions over WHTC and WHSC below EUVI limit. Results from some limited heavy-duty vehicle tests showed sufficient passive soot burn on highway but some build up and increase in pressure drop in urban driving. The aftertreatment volume and mass reduction potential reported in [77] was 52 and 48 %, respectively.

Tang et al. [50] report on experiments of a heavy-duty aftertreatment system comprising a DOC followed by a DPF with integrated SCR functionality and an ammonia slip catalyst. The size of the DPF was 12″ diameter and 12″ in length

and the ratio of filter volume to engine displacement was 2.4. The system was designed for passive operation of the DPF and testing was done under steady state conditions as well as over the NRTC. A high deNOx efficiency was observed with values of 87 and 90 % for operation at the C20 and A100 conditions, respectively. For the hot NRTC with a soot-free filter an efficiency of 92.6 % is reported, which was increased even further to 95.5 % when 6.2 g/l soot was present. This enhancement was explained by the consumption of some of the NO_2 under the conditions of a high cycle cumulative NO_2/NO_x ratio of ~68 %. The authors also discuss the reduced passive soot oxidation compared to a conventional CSF system and discuss solutions how this could be compensated. The authors demonstrate that if the ammonia dosing is reduced from a ratio of 1.05 to 0.5, intentionally accepting a reduction in deNOx, the soot accumulation could be significantly reduced, with the balance point and steady state pressure drop being reduced by almost 50 % to a value roughly equal to the condition with no ammonia being dosed. Another approach proposed is to calibrate the engine to operation at higher NOx/PM ratios.

20.6 Summary

The integration and combination of the SCR and filter functionality into one component offer some attractive features. The packaging space as well as the number of components required for the aftertreatment can be reduced. It should be mentioned that this reduction in components and size often does not lead to a reduction in system pressure drop since the effect of catalyst coating on the pressure drop is more expressed for filters than for flow-through substrates. Another advantage, attractive especially for applications with low temperatures or cold start challenges, is the potential to move the SCR function closer to the engine. This enables higher temperatures and the potential for higher deNOx efficiencies. The benefits come at the cost of increased complexity. Examples being the competition for NO_2 by the SCR reactions and the passive soot oxidation or the trade-off that has to be made when choosing the ideal pore size, balancing between the ease to coat with high loadings, and the filtration efficiency. In addition, the thermally rougher conditions observed in filters impose more challenging requirements with respect to the thermal stability of SCR catalyst technologies.

Overall, we do expect the introduction of SCR integrated filter systems in a number of passenger car applications. The tremendous progress made in the area of catalyst and filter technologies, as well as on the system integration, are key enablers. For passenger car applications, the main benefit is the potential for higher deNOx efficiencies during cold start emission cycles. The main disadvantage of reduced passive soot oxidation is less of a concern.

For heavy-duty systems, the situation is less clear although significant research and development work have been performed over the past years. The benefit with

respect to low temperature deNOx performance is less expressed and often outweighed by the disadvantage of reduced passive soot oxidation, leading to penalties in fuel consumption. The benefit of reduced packaging space or higher system deNOx efficiency at given packaging volume might be an opportunity for some truck or non-road applications designed to meet advanced regulations.

References

1. Charlton S (2010) Meeting the US Heavy-Duty EPA 2010 Standards with Increased Customer Value. Paper presented at the SAE International Heavy-Duty Diesel Emission Symposium, 2010
2. Signer M (2012) Meeting Euro VI and EPA10 Legislation without EGR. Paper presented at the SAE Heavy Duty Diesel Emissions Control Symposium, 2012
3. Herrmann H-O (2009) Der Daimler Weg zur Erfüllung der EPA'10 Gesetzgebung. Proceedings of the MTZ-Konferenz On-/Off –Highway Engines, Friedrichshafen, 2009
4. Reuss T, Bauder R, Weiss U, Macher A, Lörch H, Pamio G-Z (2012) The New, Second-Generation Audi 3.0 V6 TDI EU6 – Powerful and Economical. Proceedings of the 21st Aachener Kolloquium Fahrzeug- und Motorentechnik, Aachen, 2012
5. Enderle C, Binz R, Vent G, Stotz M (2009) BlueTEC Technology in the New E-Class to Fulfil Future EU6 Emission Limits. Proceedings of the 18. Aachener Kolloquium Fahrzeug- und Motorentechnik, Aachen, 2009
6. Miao Y, Chen L-D, He Y, Kuo T-W (2007) Study of SCR cold start by energy method. Chemical Engineering Journal 155: 260–265.
7. Darcy P, Da Costa P, Mellottee H, Trichard J-M, Djega-Mariadassou G (2007) Kinetics of catalyzed and non-catalyzed oxidation of soot from a diesel engine. Catalysis Today 119: 252–256
8. Jeguirim M, Tschamber V, Ehrburger P (1997) Catalytic effect of Platinum on the kinetics of carbon oxidation by NO_2 and O_2. Applied Catalysis B: Environmental 76: 235–240
9. Warkins J, Heibel A, George S, Golomb N, Warren C (2011) Light Duty Filters. Paper presented at the SAE Light Duty Diesel Emissions Control Symposium, Ann Arbor, MI, 2011
10. Salvat O, Marez P, Belot G (2000) Passenger car serial application of a particulate filter system on a common rail direct injection diesel engine. SAE Technical Paper 2000-01-0473
11. Lörch H, Pamio Z G, Gomm S, Gruber M (2004) Audi′s DPF solution: the advanced catalyzed soot filter. Proceedings of the 3. International Exhaust Gas and Particulate Emissions Forum, Sinsheim, 2004
12. Kercher L, Rose D, Boger T, Cutler W A, Dorenkamp R, Duesterdiek T (2006) Application of a New Filter Material in Volkswagen′s Diesel Particulate Filter Systems. Proceedings of the 3rd Emission Control Conference, Dresden, 2006
13. Adelman B, Karkkainen A, Berke P, Rodgers D, Heibel A, Parker T, Pickles D, Tao T, Zink U (2006) Development and Application of a US-EPA ′07 Particulate Filter System for a 7.6 l I-6 Medium Duty Truck Engine. Proceedings of the 15th Aachen Kolloquium Fahrzeug- und Motorentechnik, Aachen, 2006
14. Puetz W, Tindall T (2005) EPA 2007 for Heavy Duty Engines – Rewquirements and Technology. Proceedings of the 14th Aachener Kolloquium Fahrzeug- und Motorentechnik, Aachen, 2005
15. Heibel A K, Zink U (2007) Technical Paths to Emission Regulation Compliance of Commercial Vehicles in the Next Decade based upon Solutions for EPA 2007 and EU V. MTZ Vol. **68**(8): 19–25
16. Bülte H, Schiffgens H-J, Broll P, Schraml S (2009) Exhaust Aftertreatment Concepts for Engines in Mobile Machinery According the Legislation of US Tier 4 and EU Step IV

Technologies and Applications. Proceedings of the 18. Aachener Kolloquium Fahrzeug- und Motorentechnik, Aachen, 2009
17. Boger T, He S, Collins T A, Heibel A K, Beall D, Remy C (2011) A Next Generation Cordierite Diesel Particle Filter with Significantly Reduced Pressure Drop. SAE Int. J. Engines **4**(1): 902–912
18. Boger T, Rose D, Cutler W A, Heibel A K, Tennent D L (2005) Untersuchung der Eigenschaften neuer Dieselpartikelfilter. MTZ Vol. **66**(9): 660–669
19. Boger T, Jamison J A, Warkins J L, Golomb N A, Warren C JHeibel A K (2010) Next Generation Aluminum-Titanate Material to Meet Upcoming EU6 Emissions Legislation Requirements. Proceedings of the 19. Aachener Kolloquium Fahrzeug- und Motorentechnik, Aachen, 2010
20. Mizutani T, Ito M, Masukawa N, Ichikawa S, Yuuki K, Kurachi H, Toyoshima T, Ito T, Lappas I, Schaefer-Sindlinger A, Vogt C D (2006) The study for structural design of the segmented SiC-DPF. SAE Technical Paper 2006-01-1527
21. Ohno K, Shimato K, Taokam N, Santae H, Ninomiya T, Komori T, Salvat O (2000) Characterization of SiC-DPF for Passenger Car. SAE Technical Paper 2000-01-0185
22. Young D M, Hickman D L, Bhatia G, Gunasekaran N (2004) Ash storage concept for diesel particulate filters. SAE Technical Paper 2004-01-0948
23. Nova I, Bounechada D, Maestri R, Tronconi E, Heibel A K, Collins T A, Boger T (2011) Influence of the Substrate Properties on the Performances of NH3-SCR Monolithic Catalysts for the Aftertreatment of Diesel Exhaust: An Experimental and Modeling Study. Ind. Eng. Chem. Res., **50** (1): 299–309
24. Konstandopoulos A G, Johnson J H (1989) Wall-flow diesel particulate filters – Their pressure drop and collection efficiency. SAE Technical Paper 890405
25. Konstandopoulos A G (2003) Flow resistance descriptors for diesel particulate filters: Definitions, measurements and testing. SAE Technical Paper 2003-01-0846
26. Mansoudi M, Heibel A, Then P M (2000) Predicting pressure drop of wall-flow diesel particulate filters – Theory and experiment. SAE Technical Paper 2000-01-0184
27. Konstandopoulos A G, Skaperdas E, Masoudi M (2001) Inertial contributions to the pressure drop of diesel particulate filters. SAE Technical Paper 2001-01-0909
28. Gaiser G, Mucha P (2004) Prediction of pressure drop in diesel particulate filters considering ash deposit and partial regenerations. SAE Technical Paper 2004-01-0158
29. Tien C, Ramarao B V (2007) Granular Filtration of Aerosols and Hydrosols. Elsevier
30. Schermerhorn A P, Khodosevich K, Joshi A, Boger T (2012) Detailed Simulation of Exhaust Flow and Deposition of Soot Particles in Porous Particulate Filter Walls. FILTRATION 12(4): 246–256
31. Konstandopolous A G, Kostoglou M, Vlachos N, Kladopoulou E (2005) Progress in Diesel Particulate Filter Simulation. SAE Technical Paper 2005-01-0946
32. Tandon P, Rosner D E (1995) Translational Brownian Diffusion Coefficient of Large (Multiparticle) Suspended Aggregates. Ind. Eng. Chem. Res. **34**: 3265–3277
33. Heibel A K, Bhargava R (2007) Advanced Diesel Particulate Filter Design for Lifetime Pressure Drop Solution in Light Duty Applications. SAE Technical Paper 2007-01-0042
34. Bollerhoff T, Markomanolakis I, Koltsakis G (2012) Filtration and regeneration modeling for particulate filters with inhomogeneous wall structure. Catalysis Today **188:** 24–31
35. Tandon P, Heibel A, Whitmore J, Kekre N, Chithapragda K (2010) Measurement and Prediction of Filtration Efficiency Evolution of Soot Loaded Diesel Particulate Filters. Chem. Eng. Sci. 65: 4751–4760
36. Zhong D, He S, Tandon P, Moreno M, Boger T (2012) Measurement and Prediction of Filtration Efficiency Evolution of Soot Loaded Diesel Particulate Filters. SAE Technical Paper 2012-01-0363
37. Messerer A, Niessner R, Pöschl U (2006) Comprehensive kinetic characterization of the oxidation and gasification of model and real diesel soot by nitrogen oxides and oxygen under engine exhaust conditions: Measurement, Langmuir-Hinshelwood, and Arrhenius parameters. Carbon **44:** 307–324

38. Neeft J P A, Nijhuis T X, Smakman E, Makkee M, Moulijn J A (1997) Kinetics of the oxidation of diesel soot. Fuel **76**(12): 1129–1136
39. Yezerets A, Currier N W, Kim D H, Eadler H A, Epling W S, Peden C H F (2005) Differential kinetic analysis of diesel particulate matter (soot) oxidation by oxygen using a step-response technique. Applied Catalysis B: Environmental **61:** 120–129
40. Jacquot F, Logie V, Brilhac J F, Gilot P (2002) Kinetics of the oxidation of carbon black by NO_2 – Influence of the presence of water and oxygen. Carbon **40:** 335–343
41. Stanmore B R, Brilhac J F, Gilot P (2001) The oxidation of soot: A review of experiments, mechanisms and models. Carbon **39:** 2247–2268
42. Mercury D (2007) GMPT Approach to After-treatment Calibration Control. Proceedings of the SAE TopTec "Optimizing Powertrain: Future Improvements through Control Symposium", Turin June 12-14, 2007
43. Dollmeyer T A, Vittorio D A, Grana T A, Katzenmeyer J R, Charlton S J (2007) Meeting the US 2007 Heavy-Duty Diesel Emission Standards - Designing for the Customer. SAE Technical Paper 2007-01-4170
44. Becker C, Reinsch B, Strobel M, Frisse H-P, Fritsch A (2008) Particulate Filter Made of Cordierite - Design and Regeneration Management. MTZ **69**(6): 20–26
45. Boger T, Rose D, Tilgner I-C, Heibel A K (2009) Regeneration Strategies for an Enhanced Thermal Management of Oxide Diesel Particulate Filter. SAE Int. J. Fuels Lubr. 1(1):162–172. doi:10.4271/2008-01-0328.
46. Rose D, Boger T (2009) Different Approaches to Soot Estimation as Key Requirement for DPF Applications. SAE Technical Paper 2009-01-1262
47. Mandel R, Meißner R, Wenninger G, Fekete N (2010) Anwendung eines echtzeitfähigen chemo-physikalischen Modells zur gegendruckbasierten DPF-Rußbeladungserkennung. Proceedings of the 8. FAD Konferenz, Dresden, 2010
48. Meißner R, Mandel R, Wenninger G, Fekete N, Krutsch B, Kern M (2008) Auswirkungen der Dieselrußoxidation auf die gegendruckbasierte DPF-Rußbeladungserkennung. Proceedings of the 6. FAD Konferenz, Dresden, 2008
49. Zelenka P, Yoo S-B, Kim W, Lee K-M (2006) Challenges and solutions of diesel particulate filter applications. Proceedings of the 18th Int. AVL "Engine & Environment" Conference, Graz, 2006
50. Tang W, Youngren D, SantaMaria M, Kumar S (2013) On-Engine Investigation of SCR on Filters (SCRoF) for HDD Passive Applications. SAE Int. J. Engines Vol. **6**(2). doi:10.4271/2013-01-1066
51. George S, Warkins J, Golomb N, Warren C, Heibel K, Rose D (2012) A New Generation High Porosity DuraTrap® AT for Integration of DeNOx Functionalities. Proceedings of the 21st Aachener Kolloquium Fahrzeug- und Motorentechnik, Aachen, 2012
52. Stiebels S (2011) Reducing Emissions with Smart Catalyst Technologies. Paper presented at the SAE Light Duty Diesel Emissions Control Symposium, Ann Arbor, MI, 2011
53. Schrade F, Brammer M, Schaeffner J, Langeheinecke K, Kraemer L (2012) Physico-Chemical Modeling of an Integrated SCR on DPF (SCR/DPF) System. SAE Int. J. Engines Vol. **5**(3). doi:10.4271/2012-01-1083
54. Rose D, Pittner A, Jaskula C, Boger T, Glasson T, DaCosta V M (2007) On Road Durability and Field Experience Obtained with an Aluminum Titanate Diesel Particulate Filter. SAE Technical Paper 2007-01-1269
55. Bisset E J (1984) Mathematical model of the thermal regeneration of wall-flow monolith diesel particulate filter. Chem.Eng.Sci. **39:** 1233–1244
56. Watling T C, Ravenscroft M R, Avery G (2012) Development, validation and application of a model for an SCR catalyst coated diesel particulate filter. Catalysis Today **188:** 32–41
57. Konstandopoulos A G, Kostoglou M, Housiada P (2003) Multichannel simulation of regeneration of in honeycomb monolithic diesel particulate filters. Chem.Eng.Sci. **58:** 3273–3283
58. Haralampous O A, Koltsakis G (2004) Oxygen diffusion modeling in diesel particulate filter regeneration. AIChE Journal **50**(9): 2008–2019

59. Konstandopoulos A G, Kostoglou M, Vlachos N, Kladopoulou E (2005) Progress in diesel particulate filter simulation. SAE Technical Paper 2005-01-0946
60. Schejbal M, Štěpánek J, Marek M, Kočí P, Kubíček M (2010) Modeling of soot oxidation by NO2 in various types of diesel particulate filters. Fuel **89:** 2365–2375
61. Dardiotis C K, Haralampous O A, Koltsakis G (2008) Catalytic oxidation in wall-flow reactors with zoned coating. Chemical Engineering Science **63:** 1142–1153
62. Schejbal M, Marek M, Kubíček M, Kočí P (2009) Modeling of diesel filters for particulates removal. Chemical Engineering Journal **154:** 219–230
63. Lee J H, Paratore M J, Brown D B (2009) Evaluation of Cu-Based SCR/DPF Technology for Diesel Exhaust Emission Control. SAE Int. J. Fuels Lubr. Volume 1 (1): 96–101
64. He Y, Brown D B, Lu S, Paratore M J, Li J (2009) Opportunities and Challenges for Blended 2-Way SCR/DPF Aftertreatment Technologies. SAE Technical Paper 2009-01-0274
65. Cavataio G, Girard J W, Lambert C K (2009) Cu/Zeolite SCR on High Porosity Filters: Laboratory and Engine Performance Evaluations. SAE Technical Paper 2009-01-0897
66. Guo G, Warner J, Cavataio G, Dobson D, Badillo E, Lambert C (2010) The Development of Advanced Urea-SCR Systems for Tier 2 Bin 5 and Beyond Diesel Vehicles. SAE Technical Paper 2010-01-1183
67. Harth K (2012) Compact catalytic converter systems for future emissions standards. MTZ Vol. **73**(9): 10–14
68. Boorse S, Dieterle M, Voss K, Stiebels s, Wendt C, Neubauer T (2010) Two in one: SCR on Filter. Paper presented at the DEER Conference, 2010
69. Dieterle M, Boorse S, Voss K, Stiebels S, Wendt C, Neubauer T (2010) Two in one: SCR on Filter. Proceedings of the 3rd MinNOx Conference, Berlin, 2010
70. Grisstede I, Franoschek S, Seyler M, Hoyer R, Noack H, Basso S, Müller W (2012) Robust NOx After Treatment Systems for Diesel Pass-Cars Beyond EU6. Proceedings of the 21. Aachener Kolloquium Fahrzeug- und Motorentechnik, Aachen, 2012
71. Ballinger T, Cox J, Konduru M, De D, Manning W, Andersen P (2009) Evaluation of SCR Catalyst Technology on Diesel Particulate Filters. SAE Int. J. Fuels Lubr., Vol. **2**(1): 369–374
72. Neußer H-J, Kahrstedt J, Jelden H, Dorenkamp R, Düsterdiek T (2013) The EU6 Engines based on the Modular Diesel System of Volkswagen – Innovative Exhaust Gas Purification Near the Engine for Further Minimization of NOx and CO_2. Proceedings of the 34. Internationales Wiener Motorensymposium, Vienna, 2013
73. Oladipo B, Bailey O, Price K, Balzan N, Kaul S (2008) Simplification of Diesel Emission Control System Packaging Using SCR Coated on DPF. Paper presented at the 14th DEER Conference, 2008
74. Naseri M, Chatterjee S, Castagnola M, Chen H-Y, Fedeyko J, Hess H, Li, J (2011) Development of SCR on Diesel Particulate Filter System for Heavy Duty Applications. SAE Int. J. Engines, Vol. **4**(1): 1798–1809
75. Tan J, Solbrig C, Schmieg S J (2011) The Development of Advanced 2-Way SCR/DPF Systems to Meet Future Heavy-Duty Diesel Emissions. SAE Technical Paper 2011-01-1140
76. Döring A, Emmerling G, Rothe D (2012) Downsizing of the EUVI exhaust aftertreatment components to fit into the Euro III silencer. Proceedings of the 33. Internationales Wiener Motorensymposium, Vienna, 2012
77. Emmerling G, Döring A, Rothe D (2012) "SCR on DPF" for commercial vehicles – advantages and risks. Proceedings of the 6th Emission Control Conference, Dresden, 2012